Unexpected effects of third-order cross-terms in heteronuclear spin systems under simultaneous radio-frequency irradiation and magic-angle spinning NMR

Andrew S. Tatton,[1] Ilya Frantsuzov,[2] Steven P. Brown,[1] and Paul Hodgkinson[2,a)]
[1]*Department of Physics, University of Warwick, Coventry CV4 7AL, United Kingdom*
[2]*Department of Chemistry, Durham University, South Road, Durham DH1 3LE, United Kingdom*

(Received 9 November 2011; accepted 25 January 2012; published online 24 February 2012)

We recently noted [R. K. Harris, P. Hodgkinson, V. Zorin, J.-N. Dumez, B. Elena, L. Emsley, E. Salager, and R. Stein, Magn. Reson. Chem. **48**, S103 (2010)] anomalous shifts in apparent ^{1}H chemical shifts in experiments using ^{1}H homonuclear decoupling sequences to acquire high-resolution ^{1}H NMR spectra for organic solids under magic-angle spinning (MAS). Analogous effects were also observed in numerical simulations of model ^{13}C,^{1}H spin systems under homonuclear decoupling and involving large ^{13}C,^{1}H dipolar couplings. While the heteronuclear coupling is generally assumed to be efficiently suppressed by sample spinning at the magic angle, we show that under conditions typically used in solid-state NMR, there is a significant third-order cross-term from this coupling under the conditions of simultaneous MAS and homonuclear decoupling for spins directly bonded to ^{1}H. This term, which is of the order of 100 Hz under typical conditions, explains the anomalous behaviour observed on both ^{1}H and ^{13}C spins, including the fast dephasing observed in ^{13}C{^{1}H} heteronuclear spin-echo experiments under ^{1}H homonuclear decoupling. Strategies for minimising the impact of this effect are also discussed. © *2012 American Institute of Physics*. [http://dx.doi.org/10.1063/1.3684879]

I. INTRODUCTION

The line broadening due to non-commuting homonuclear ^{1}H-^{1}H dipolar couplings associated with the extensive network of dipolar-coupled protons formed by the packing of organic molecules in the solid state represents a major challenge for ^{1}H solid-state NMR spectroscopy.[1] The ability of radio-frequency (RF) irradiation to counteract the effect of homonuclear dipolar couplings was demonstrated in the 1960s in the Lee-Goldburg[2] and WAHUHA[3] methods for static samples and in the 1970s in the combined rotation and multiple-pulse spectroscopy (CRAMPS) (Ref. 4) approach under magic-angle spinning (MAS). However, it is only with the development of ^{1}H homonuclear decoupling schemes suitable for application under moderate to fast MAS frequencies, e.g., Frequency-Switched Lee-Goldburg (FSLG),[5] Phase-Modulated Lee-Goldburg (PMLG),[6] and DUMBO,[7] coupled with advances in RF consoles, that such experiments have started to be more widely employed.[8,9] For example, ^{13}C,^{1}H heteronuclear correlation (HETCOR) experiments at moderate to fast MAS frequencies[10,11] have been widely applied to a variety of significant material types, such as proteins,[12,13] pharmaceuticals,[14,15] silica-supported catalytic complexes,[16,17] organic-templated microporous materials,[18] inorganic-organic hybrid materials,[19] as well as chemical problems, such as the characterisation of weak hydrogen bonding in sugars[20] and the solution of structures from powder diffraction data.[21] Heteronuclear ^{13}C{^{1}H} spin-echo experiments employing ^{1}H homonuclear decoupling during the spin-echo evolution periods have also been presented and shown to be applicable for spectral editing and the determination of $^{1}J_{CH}$ couplings for typical organic compounds,[22,23] including the use of measured J couplings to determine the conformation of surface-absorbed catalytic species.[24]

This paper investigates two experimental phenomena associated with the application of homonuclear ^{1}H decoupling in heteronuclear ^{13}C,^{1}H solid-state MAS NMR; firstly, changes in the apparent ^{1}H chemical shift of correlation peaks in ^{1}H,^{13}C two-dimensional experiments depending on whether there is or is not a one-bond ^{13}C-^{1}H dipolar coupling, and secondly, the observation of a much faster dephasing in a ^{13}C{^{1}H} heteronuclear spin-echo experiment under homonuclear ^{1}H decoupling as compared to heteronuclear ^{1}H decoupling. An analytical description is presented that, supported by numerical simulations, shows that these two phenomena have a common explanation in terms of third-order cross terms involving the ^{13}C,^{1}H heteronuclear dipolar coupling.

II. EXPERIMENTAL PHENOMENA

Figure 1(c) shows the overlay of two ^{13}C,^{1}H HETCOR spectra of terbutaline sulfate (TBS) form B, obtained at 500 MHz ^{1}H NMR frequency using cross-polarisation mixing times of 150 and 350 μs under otherwise identical conditions (full experimental details can be found in Ref. 25). As noted in the original reference, small, but consistent, discrepancies were observed between apparent ^{1}H shifts obtained from the positions of long- vs. short-range correlation peaks. The figure shows a region where these

a)Author to whom correspondence should be addressed. Electronic mail: paul.hodgkinson@durham.ac.uk.

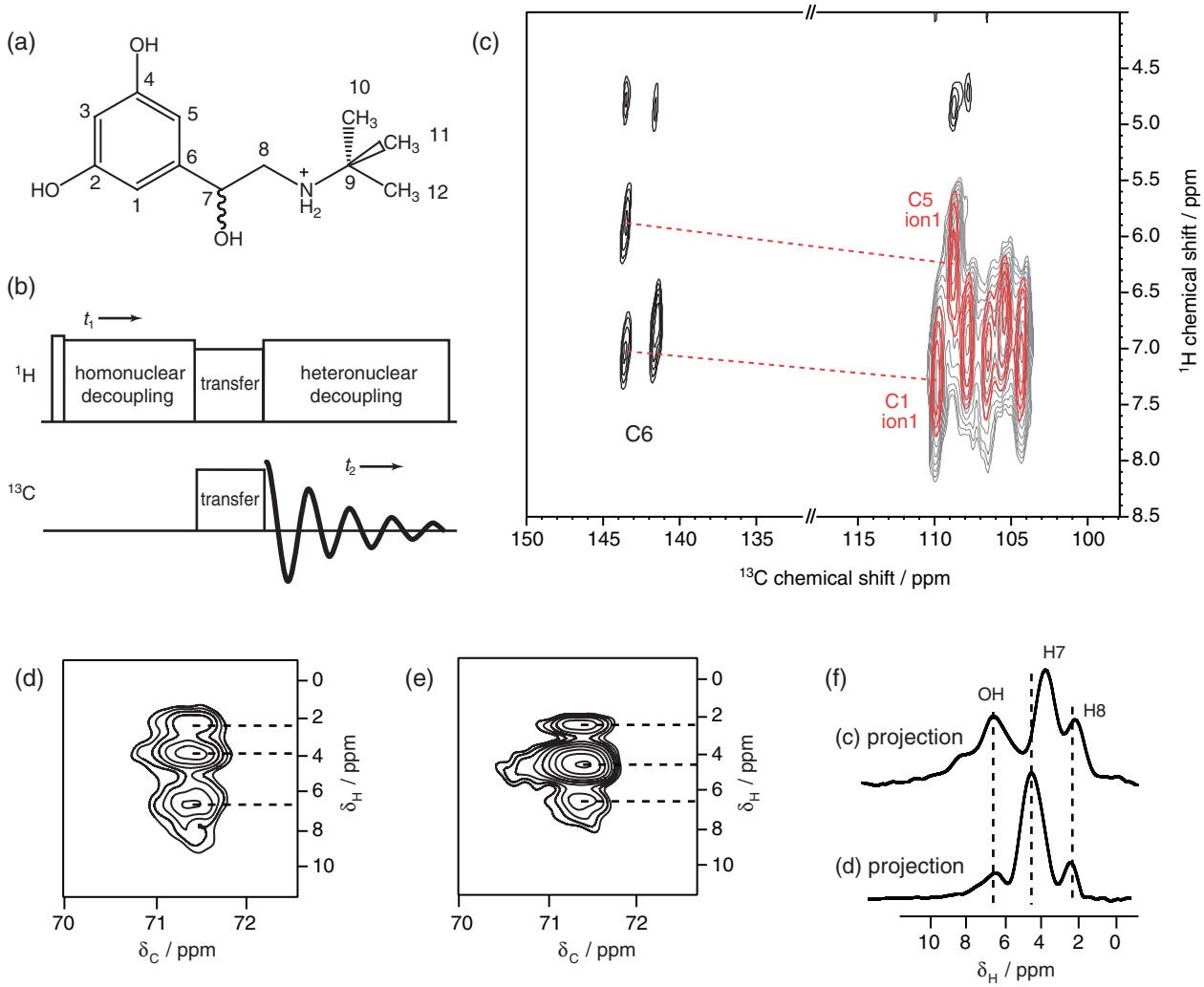

FIG. 1. (a) Schematic of the terbutaline ion. (b) Schematic ^{13}C,^{1}H HETCOR pulse sequence, where heteronuclear coherence transfer can be achieved by using CP (as here), LG-CP,[11] or refocused INEPT.[23] (c) Superposition of the same region from ^{13}C,^{1}H HETCOR (500 MHz, 12.5 kHz MAS) spectra of terbutaline sulfate form B recorded using contact times of (red) 150 μs and (grey/black) 350 μs. The long-range cross peaks (black) involving the two C6 resonances have subtly different apparent ^{1}H shifts compared to short-range correlations involving the same hydrogens (red). The short-range one-bond CH correlation peaks at the two times are directly superimposable (the peaks from the long contact time experiment are greyed out for clarity). (d and e) Expansion of the C7 region of HETCOR (at 399.88 MHz, 8 kHz MAS) spectra of diterbutaline sulfate diacetic acid solvate using 85 kHz FSLG decoupling on ^{1}H; (d) 1.0 ms contact time, ^{1}H transmitter at +2.2 ppm, (e) 100 μs contact time, transmitter at −2.2 ppm. (f) The short-range correlation peak to H7 is noticeably shifted by the change in decoupler offset.

effects are most evident. The short-range correlation peaks are exactly superimposable, confirming that any shifts cannot be explained by differences in referencing, but the ^{1}H chemical shifts obtained by projecting the positions of the peak maxima on to the ^{1}H axis are not the same. This is shown explicitly for the ^{1}H attached to C1 (of TBS ion 1) observed via the short-range correlation (overlaid grey and red peaks) compared to the long-range correlation to C6 (ion 1). The lines connecting peak maxima of the correlation peaks for the same-proton correlations are clearly not parallel to the horizontal axis. Similar shifts have been observed in HETCOR spectra acquired at different decoupler offsets for a different solid form of terbutaline, see Figs. 1(d) and 1(e). The long-range correlation peaks are unaffected by the change in decoupler offset, while the short-range correlation peak between C7 and its directly bonded hydrogen (H7) is shifted by about 0.4 ppm (at a ^{1}H NMR frequency of 399.88 MHz; full details can be found in Ref. 26).

Related effects may be observed for dilute spins, such as ^{13}C, when homonuclear decoupling is applied to the ^{1}H spins. Figure 2 shows the results (solid lines) of spin-echo experiments used to measure the $^1J_{CH}$ couplings for the CH and CH_3 resonances of L-alanine. eDUMBO-1_{22}[27] ^{1}H homonuclear decoupling was applied during the echo periods (each of duration τ) to reduce the dephasing due to the ^{1}H dipolar coupling network; full experimental details are given in the supplementary information.[65] The solid curves show fits of the peak areas as a function of 2τ to $\cos 2\pi J\tau$ (CH) and $\cos^3 2\pi J\tau$ (CH_3) functions exponentially damped by a decay with time constant T_2' (fitted values shown). Although the spin-echo curves fit reasonably well to these functions, the fitted decay constants are relatively short in comparison to those observed when heteronuclear decoupling is applied, limiting the accuracy with which the J values can be determined. This is demonstrated in Fig. 2 using data (fitted by dashed lines) acquired with SPINAL-64 *heteronuclear* decoupling[28] during

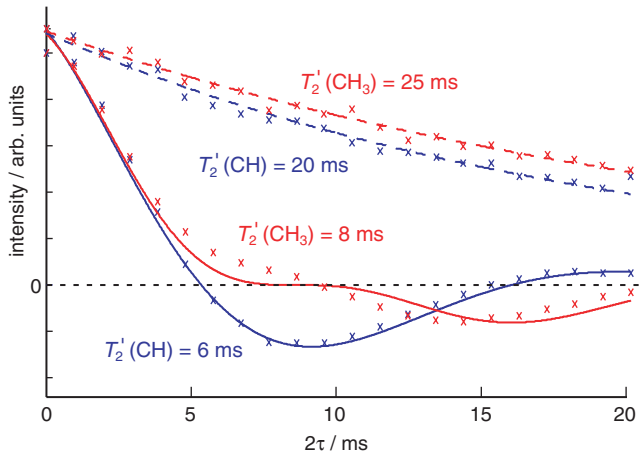

FIG. 2. Spin-echo decays for the CH and CH_3 carbons of L-alanine using (solid lines) windowless eDUMBO-1_{22} ^{1}H homonuclear decoupling ($\nu_{rf} = 120$ kHz) and (dashed lines) SPINAL-64 ^{1}H heteronuclear decoupling ($\nu_{rf} = 100$ kHz) during the rotation-synchronised τ echo periods. The ^{1}H NMR frequency was 599.44 MHz and the MAS spinning rate 20.833 kHz. 180° pulses were applied to both ^{1}H and ^{13}C channels and the ^{13}C peak areas measured at the end of the τ-π-τ period. Figures with each curve show the T_2' values obtained by fitting.

the spin-echo period. The fitted time constants, which are consistent with previous experimental observations,[29] are about three times larger than those observed with homonuclear decoupling using the same ^{1}H RF power.

One significant distinction between the two spin-echo experiments shown in Fig. 2 is the non-zero scaling of the heteronuclear dipolar coupling when homonuclear decoupling is used. It is widely assumed that the heteronuclear dipolar coupling is averaged out by magic-angle spinning and so the only active coupling should be a small (scaled) $^1J_{CH}$ coupling. However, we show below that the heteronuclear dipolar coupling is not innocent and is largely responsible both for the rapid decay of the spin-echo curves in Fig. 2 and the peak shifts shown in Fig. 1.

III. ANALYSIS

These effects were suspected to have a common origin in the large heteronuclear dipolar interaction between a ^{13}C and its directly bonded ^{1}H. We consider a heteronuclear spin pair under magic-angle spinning, using I to denote the spin subject to RF decoupling and S for the heteronucleus. We consider initially simple Lee-Goldburg decoupling, i.e., using off-resonance irradiation to rotate the I spin magnetisation about an axis inclined at the magic angle with respect to B_0.

The relevant spin Hamiltonian is therefore

$$\hat{H}(t) = [2\omega_D(t) + \omega_J]\,\hat{I}_z\hat{S}_z + [\omega_I(t) + \Delta_{off}]\,\hat{I}_z + \omega_{rf}\hat{I}_x, \tag{1}$$

where ω_D is the heteronuclear dipolar coupling between I and S and ω_I is the I spin chemical shift relative to the on-resonance I spin RF frequency (these are time dependent due to MAS), $\omega_J = 2\pi J$ is the isotropic J coupling between I and S (in angular frequency units), Δ_{off} is the offset from the I spin detection frequency, and ω_{rf} is the I spin nutation frequency (on resonance). The S spin chemical shift may be ignored as its Hamiltonian commutes with $\hat{H}$.

The problem can be simplified using a tilted frame whose z axis lies along the spin-lock axis

$$\hat{I}_x \rightarrow \cos\theta\,\hat{I}'_x + \sin\theta\,\hat{I}'_z \qquad \hat{I}_z \rightarrow \cos\theta\,\hat{I}'_z - \sin\theta\,\hat{I}'_x, \tag{2}$$

where the tilt angle θ is chosen such that $\omega_{rf} = \Delta_{off}\tan\theta$. θ is the magic angle, θ_m, for perfectly adjusted Lee-Goldburg decoupling. Equation (1) then becomes

$$\hat{H}'(t) = [(2\omega_D(t) + \omega_J)\hat{S}_z + \omega_I(t)](\cos\theta\,\hat{I}'_z - \sin\theta\,\hat{I}'_x) + \omega_{eff}\hat{I}'_z, \tag{3}$$

where the effective precession frequency is $\omega_{eff} = \omega_{rf}/\sin\theta$.

The Hamiltonian is block diagonal with respect to the S spin state, and so the analysis can be simplified by working in the subspaces corresponding to the two S spin states

$$\hat{H}_\pm(t) = \omega_\pm(t)(\cos\theta\,\hat{I}'_z - \sin\theta\,\hat{I}'_x) + \omega_{eff}\hat{I}'_z, \tag{4}$$

where the effective I spin frequency is $\omega_\pm(t) = \omega_I(t) \pm (\omega_D(t) + \omega_J/2)$.

A. Observation via heteronucleus

Focussing initially on the heteronucleus, the S spin signal at multiples, N, of the RF cycle time, τ_c, is given by

$$S(N\tau_c) = \mathrm{tr}(U(\tau_c)^N\,\hat{S}_x\,U(\tau_c)^{\dagger N}\,\hat{S}_+), \tag{5}$$

where $U(\tau_c)$ is the propagator over one period of the RF. This problem is expressed in terms of propagators evaluated in the sub-space of the I spins for the two states of the S spin,[30] $U_\pm$, with

$$U(\tau_c) = \begin{pmatrix} U_+ & \mathbf{0} \\ \mathbf{0} & U_- \end{pmatrix}. \tag{6}$$

Equation (5) becomes[30]

$$S(N\tau_c) = \mathrm{tr}[(U_-U_+^\dagger)^N]/2. \tag{7}$$

Note that perfect decoupling would correspond to $U_+ = U_-$, i.e., the same evolution irrespective of the S spin state.

Using a similar approach to Waugh,[31] the propagators can be expressed in terms of the eigenvector matrices $V_\pm$ and eigenvalues $\lambda_\pm$ which diagonalise them. Hence

$$\mathrm{tr}[(U_-U_+^\dagger)^N] = \mathrm{tr}[V_-e^{i\lambda_-N}V_-^\dagger V_+e^{-i\lambda_+N}V_+^\dagger]. \tag{8}$$

In the limit of strong decoupling, the two propagators are very similar and $V_+ \approx V_-$. Hence

$$\mathrm{tr}[(U_-U_+^\dagger)^N] \approx \sum_{j=1,2} e^{i(\lambda_{-,j}-\lambda_{+,j})N} = \sum_{j=1,2} e^{-i\Omega_jN}, \tag{9}$$

which corresponds to a sum of two oscillation frequencies at the differences of corresponding eigenvalues of the effective Hamiltonian over the RF period, $\Omega_j = \lambda_{+,j} - \lambda_{-,j}$. The eigenvectors only modify the transition amplitudes and can be ignored in the strong decoupling limit.[32]

In common with recent theoretical analyses of heteronuclear decoupling,[33–36] we use Floquet theory to express the time-dependent Hamiltonian in non-time-dependent form.

Since the RF irradiation is time independent, it is sufficient to expand the Hamiltonian with respect to a single Floquet mode corresponding to the sample rotation, with Fourier modes $-2, \ldots, +2$,

$$\hat{H}_{\pm}(t) = \sum_{n=-2}^{2} \hat{H}_{\pm}^{(n)} e^{in\omega_r t} \tag{10}$$

$$= \omega_{\text{eff}} \hat{I}'_z + \sum_{n=-2}^{2} \omega_{\pm}^{(n)} (\cos\theta \hat{I}'_z - \sin\theta \hat{I}'_x) e^{in\omega_r t}, \tag{11}$$

where $\hat{H}_{\pm}^{(n)}$ is the nth term in the Fourier series expansion of Eq. (4), and ω_r is the spinning frequency (as an angular frequency). The distinct Fourier coefficients of the NMR interactions under MAS are

$$\omega_{\pm}^{(0)} = \Omega_{\text{I}} \pm \omega_{\text{J}}/2, \tag{12}$$

$$\omega_{\pm}^{(1)} = \omega_{\text{I}}^{(1)} \pm \omega_{\text{D}}^{(1)}, \tag{13}$$

$$\omega_{\pm}^{(2)} = \omega_{\text{I}}^{(2)} \pm \omega_{\text{D}}^{(2)}, \tag{14}$$

where $\omega_{\Lambda}^{(n)}$ is the order n coefficient of the tensor for the interaction Λ in the rotor frame. $\omega_{\text{D}}^{(n)}$ and $\omega_{\text{I}}^{(n)}$ are proportional to the dipolar coupling constant, D, and the I spin chemical shift anisotropy (CSA), respectively; full expressions for $\omega_{\Lambda}^{(n)}$ can be found in Appendix A of Ref. 37. Note the symmetry relationships $\omega_{\Lambda}^{(2)} = \omega_{\Lambda}^{(-2)}$ and $\omega_{\Lambda}^{(1)} = -\omega_{\Lambda}^{(-1)*}$, and that $\omega_{\text{D}}^{(0)} = 0$ and $\omega_{\text{I}}^{(0)} = \Omega_{\text{I}}$ at the magic angle, where Ω_{I} is the I spin isotropic frequency relative to the on-resonance RF frequency.

The zero-order term in the Fourier series expansion is

$$\hat{H}_{\pm}^{(0)} = \omega_{\text{eff}} \hat{I}'_z + \omega_{\pm}^{(0)} (\cos\theta \hat{I}'_z - \sin\theta \hat{I}'_x) \tag{15}$$

$$= \begin{pmatrix} (\omega_{\pm}^{(0)} \cos\theta + \omega_{\text{eff}})/2 & -\omega_{\pm}^{(0)} \sin\theta/2 \\ -\omega_{\pm}^{(0)} \sin\theta/2 & -(\omega_{\pm}^{(0)} \cos\theta + \omega_{\text{eff}})/2 \end{pmatrix}. \tag{16}$$

Following the notation of Leskes *et al.*,[38] the Floquet Hamiltonian is written

$$\hat{H}_{\pm}^{\text{F}} = \omega_r \hat{N} + \sum_{n=-2}^{2} \hat{H}_{\pm}^{(n)} \otimes \hat{F}_n, \tag{17}$$

where the Fourier operators acting on the Fourier mode are

$$\hat{N}|m\rangle = m|m\rangle, \qquad \hat{F}_n|m\rangle = |n+m\rangle. \tag{18}$$

The matrix representation of Eq. (17) is an infinite matrix of the form

$$\hat{H}_{\pm}^{\text{F}} = \begin{pmatrix} \ddots & \vdots & \vdots & & & & \\ \cdots & \hat{H}_{\pm}^{(0)} + 2\omega_r \boldsymbol{I} & \hat{H}_{\pm}^{(1)} & \hat{H}_{\pm}^{(2)} & & & \\ \cdots & \hat{H}_{\pm}^{(-1)} & \hat{H}_{\pm}^{(0)} + \omega_r \boldsymbol{I} & \hat{H}_{\pm}^{(1)} & \hat{H}_{\pm}^{(2)} & & \\ & \hat{H}_{\pm}^{(-2)} & \hat{H}_{\pm}^{(-1)} & \hat{H}_{\pm}^{(0)} & \hat{H}_{\pm}^{(1)} & \hat{H}_{\pm}^{(2)} & \\ & & \hat{H}_{\pm}^{(-2)} & \hat{H}_{\pm}^{(-1)} & \hat{H}_{\pm}^{(0)} - \omega_r \boldsymbol{I} & \hat{H}_{\pm}^{(1)} & \cdots \\ & & & \hat{H}_{\pm}^{(-2)} & \hat{H}_{\pm}^{(-1)} & \hat{H}_{\pm}^{(0)} - 2\omega_r \boldsymbol{I} & \cdots \\ & & & & \vdots & \vdots & \ddots \end{pmatrix}, \tag{19}$$

where $\boldsymbol{I}$ is a 2×2 identity matrix. Only the non-zero terms of $\hat{H}_{\pm}^{\text{F}}$, corresponding to Fourier modes up to $|n| = 2$, are indicated, all other matrix elements are zero.

The transformation into the titled rotating frame has ensured that the Hamiltonian is diagonally dominant (i.e., the diagonal term $\omega_{\text{eff}} \hat{I}'_z$ of Eq. (3) is assumed to be much larger than the NMR interactions). However further simplification is not possible since $\omega_r \sim \omega_{\pm}$. This contrasts to previous work where van Vleck transformations were used to determine successively more accurate approximations to the overall effective Hamiltonian.[33,39–44]

However, it is straightforward to use non-degenerate perturbation theory to estimate the eigenvalues of $\hat{H}^{\text{F}}$, provided the resonance conditions observed in Fig. 9 are avoided—these would introduce degeneracies along the diagonal of $\hat{H}^{\text{F}}$. The eigenvalues will be of the form

$$\lambda_{\nu,i} = \lambda_i + \nu\omega_r, \tag{20}$$

where $\nu = -\infty \ldots \infty$ is the index over the Floquet mode, and the "base" eigenvalues λ_i^{F} can be determined from the central block of $\hat{H}^{\text{F}}$, which is $\hat{H}_{\pm}^{(0)}$ in Eq. (19). The eigenvalues associated with $\nu \neq 0$ correspond to spinning sidebands, whose intensity can be ignored away from resonance conditions.

Dividing the Hamiltonian into a diagonal zero-order component, $\hat{H}_{\pm}^{0}$ and an off-diagonal perturbation term, $\hat{V}_{\pm}$, the eigenvalues to first order (i.e., the diagonal terms of $\hat{H}_{\pm}^{(0)}$, Eq. (16)) are

$$\lambda_{\pm,1}^{\text{I}} = (\omega_{\pm}^{(0)} \cos\theta + \omega_{\text{eff}})/2 \quad \lambda_{\pm,2}^{\text{I}} = -(\omega_{\pm}^{(0)} \cos\theta + \omega_{\text{eff}})/2, \tag{21}$$

where the superscript Roman numerals (I in Eq. (21), II and III below) indicate the perturbation order.

Hence the dominant frequencies in the spectrum, $\Omega_j = \lambda_{+,j} - \lambda_{-,j}$ (Eq. (9)) are to first order

$$\Omega^{\mathrm{I}}_{1,2} = \pm((\omega^{(0)}_{+} - \omega^{(0)}_{-})\cos\theta)/2 = \pm(\omega_{\mathrm{J}}/2)\cos\theta. \tag{22}$$

Note that the transition frequencies for S spin observation are symmetrical about zero frequency, hence the *splitting* to first order is

$$\Delta^{\mathrm{I}} = \left|\Omega^{\mathrm{I}}_1 - \Omega^{\mathrm{I}}_2\right|, \tag{23}$$

$$= \left|\left(\lambda^{\mathrm{I}}_{+,1} - \lambda^{\mathrm{I}}_{-,1}\right) - \left(\lambda^{\mathrm{I}}_{+,2} - \lambda^{\mathrm{I}}_{-,2}\right)\right|, \tag{24}$$

$$= 2\left|\lambda^{\mathrm{I}}_{+,1} - \lambda^{\mathrm{I}}_{-,1}\right| = 2\left|\lambda^{\mathrm{I}}_{+,2} - \lambda^{\mathrm{I}}_{-,2}\right|, \tag{25}$$

$$= |\omega_{\mathrm{J}}\cos\theta|. \tag{26}$$

As expected, this corresponds to the isotropic J coupling scaled by $\cos\theta$. Note that the restricted number of Fourier modes ($|n| \leq 2$) for this problem means that there are a finite number of non-zero elements (giving rise to correction terms) for each eigenvalue. This contrasts with problems involving time-dependent RF where the Fourier series are in general infinite.

The second-order corrections to the eigenvalues are given by

$$\lambda^{\mathrm{II}}_{\pm,i} = \sum_{j\neq i} \frac{\langle j|\hat{V}_{\pm}|i\rangle\langle i|\hat{V}_{\pm}|j\rangle}{E^{(0)}_{\pm,i} - E^{(0)}_{\pm,j}}, \tag{27}$$

where $E^{(0)}_{\pm,j} = \langle j|\hat{H}^{(0)}_{\pm}|j\rangle$ are the energies of the unperturbed states.

These correction terms have been evaluated analytically using the computer algebra system, MAPLE™.[45] The resulting second-order contribution to the splitting in the S spin spectrum is

$$\Delta^{\mathrm{II}} = \left|\Omega^{\mathrm{II}}_1 - \Omega^{\mathrm{II}}_2\right| = \frac{\sin^2\theta}{\omega_{\mathrm{eff}}}\left(4\left(\omega^{(2)}_{\mathrm{I}}\omega^{(2)}_{\mathrm{D}} - \omega^{(1)}_{\mathrm{I}}\omega^{(1)}_{\mathrm{D}}\right) + \Omega\omega_{\mathrm{J}}\right). \tag{28}$$

These are second-order cross terms that diminish inversely with the effective RF nutation frequency, ω_{eff}. The first term corresponds to the dipolar-chemical shielding anisotropy cross-term first discussed by Ernst *et al.*,[32] and the second is a correction to the scaling of ω_{J} due to deviations from the Lee-Goldburg off-resonance condition due to a non-zero offset Ω_{I}. These terms are expected to be suppressed by the frequency switching of FSLG decoupling, which effectively alternates the sign of the ω_{eff} leading to cancellation over a complete FSLG cycle. This cancellation is discussed further in Sec. III C below.

The third-order corrections to the eigenvalues are given by[46]

$$\lambda^{\mathrm{III}}_{\pm,i} = \sum_{j,k\neq i} \frac{\langle i|\hat{V}_{\pm}|j\rangle\langle j|\hat{V}_{\pm}|k\rangle\langle k|\hat{V}_{\pm}|i\rangle}{\left(E^{(0)}_{\pm,j} - E^{(0)}_{\pm,i}\right)\left(E^{(0)}_{\pm,k} - E^{(0)}_{\pm,i}\right)} - \langle i|\hat{V}_{\pm}|i\rangle \sum_{j\neq i} \frac{\langle j|\hat{V}_{\pm}|i\rangle\langle i|\hat{V}_{\pm}|j\rangle}{\left(E^{(0)}_{\pm,i} - E^{(0)}_{\pm,j}\right)^2}. \tag{29}$$

Although the number of correction terms is finite, the resulting expressions are extremely cumbersome, and can only be usefully evaluated in a narrower parameter space. Cross-terms involving the J coupling and the ^{1}H offset are assumed to be negligible. The ^{1}H CSA is assumed to be small compared to the dipolar coupling, and set to zero (as in the majority of the simulations below). We also assume that $\omega_{\mathrm{eff}} \gg \omega_r$ and then use the approximation that denominator terms involving $n\omega_r \pm \omega_{\mathrm{eff}}$ can be replaced by ω_{eff}. This approximation has to be done carefully to avoid the erroneous cancellation of several pairs of terms of the form

$$\frac{A}{\omega_r(n\omega_r - \omega_{\mathrm{eff}})} + \frac{A}{\omega_r(n\omega_r + \omega_{\mathrm{eff}})}. \tag{30}$$

These terms only truly cancel in the limit $\omega_{\mathrm{eff}}/\omega_r \to \infty$, and the general limit, i.e., $-2nA/\omega^2_{\mathrm{eff}}$, must be evaluated on the sum of matching pairs.

The third-order correction to the S spin splitting then reduces to

$$\Delta^{\mathrm{III}} = \frac{6\sin^2\theta\cos\theta}{\omega^2_{\mathrm{eff}}}\omega^{(2)}_{\mathrm{D}}\left(\omega^{(1)}_{\mathrm{D}}\right)^2. \tag{31}$$

This term will not be removed by frequency switching as it is even order with respect to ω_{eff} (cf. Fig. 3).

B. Observation via irradiated nucleus

Determination of the I spin response introduces no new principles. For a given crystallite orientation, two frequencies will be observed corresponding to the two states of the S spin, $\Omega_{\pm} = \lambda_{\pm,1} - \lambda_{\pm,2}$. To first order, these frequencies relative to the nutation frequency, ω_{eff}, are $\Omega^{\mathrm{I}}_{\pm} = \cos\theta(\Omega \pm \omega_{\mathrm{J}}/2)$, corresponding to the expected scaled offset and J coupling. The second-order corrections to the two I spin transition frequencies can be expressed in terms of an overall shift of the I spin frequency and a contribution to the frequency difference. The latter splitting contribution is identical to Eq. (28), as would be expected for a mutual interaction. The overall *shift* to second order is

$$-\frac{\sin^2\theta}{\omega_{\mathrm{eff}}}\left[\left(\omega^{(2)}_{\mathrm{D}}\right)^2 - \left(\omega^{(1)}_{\mathrm{D}}\right)^2 + \left(\omega^{(2)}_{\mathrm{I}}\right)^2 - \left(\omega^{(1)}_{\mathrm{I}}\right)^2 + \frac{\Omega^2_{\mathrm{I}}}{2} + \frac{\omega^2_{\mathrm{J}}}{8}\right]. \tag{32}$$

This contribution is odd-order with respect to the RF and so is expected to average out for FSLG decoupling.

There are a significantly greater number of third-order terms for the I spin observation, as fewer contributions cancel. Discarding terms that are odd-order with respect to the RF, i.e., those expected to be suppressed by frequency switching in FSLG, and neglecting the effects of ^{1}H CSA and the J coupling, and again assuming that $\omega_{\mathrm{eff}} \gg \omega_r$, the I spin transition frequencies to third order are

$$\Omega^{\mathrm{III}}_{\pm} = \lambda^{\mathrm{III}}_{\pm,1} - \lambda^{\mathrm{III}}_{\pm,2} = \frac{\sin^2\theta\cos\theta}{2\omega^2_{\mathrm{eff}}}\left(4\Omega_{\mathrm{I}}\left[\left(\omega^{(2)}_{\mathrm{D}}\right)^2 - \left(\omega^{(1)}_{\mathrm{D}}\right)^2\right] + \Omega^3_{\mathrm{I}} \pm 6\left(\omega^{(1)}_{\mathrm{D}}\right)^2\omega^{(2)}_{\mathrm{D}}\right). \tag{33}$$

Full expressions for the spin transition frequencies are given in the supplementary information.[65]

Hence the contribution to the splitting on the I spin spectrum is

$$\Delta^{\mathrm{III}} = \left|\Omega_{+}^{\mathrm{III}} - \Omega_{-}^{\mathrm{III}}\right| = \frac{6\sin^2\theta\cos\theta}{\omega_{\mathrm{eff}}^2}\left(\omega_{\mathrm{D}}^{(1)}\right)^2\omega_{\mathrm{D}}^{(2)}, \tag{34}$$

which is identical to the S spin correction term of Eq. (31). The midpoint of the I spin transition frequencies is shifted by a term proportional to Ω_{I}. In other words, the effective scaling factor on the I spin frequencies is modified from $\cos\theta$ to

$$\cos\theta\left(1 + \frac{\sin^2\theta}{2\omega_{\mathrm{eff}}^2}\left[4\left(\omega_{\mathrm{D}}^{(2)}\right)^2 - 4\left(\omega_{\mathrm{D}}^{(1)}\right)^2 + \Omega_{\mathrm{I}}^2\right]\right). \tag{35}$$

Since this modification of the scaling factor will be orientation dependent, it will lead to additional linebroadening and resolution loss, whose impact will increase in proportion to the offset Ω_{I}.

C. Discussion of analysis

The correction term in Eqs. (31) and (34) has a number of interesting properties. First, being a pure heteronuclear coupling term, it is not refocused by the heteronuclear spin-echo sequence used to observe the heteronuclear J coupling. Second, the $\sin^2\theta\cos\theta$ scaling factor has its maximum at $\theta = \theta_{\mathrm{m}}$, i.e., at the conditions required for efficient homonuclear decoupling, but it is zero for on-resonance CW decoupling; this helps to explain why it has not been discussed in the context of earlier studies of heteronuclear decoupling. Moreover, the functional dependence of the product $\omega_{\mathrm{D}}^{(2)}(\omega_{\mathrm{D}}^{(1)})^2$ on the angle β between the principal axis of heteronuclear dipolar coupling and the rotation axis is

$$\Delta^{\mathrm{III}} \propto d_{2,0}^{(2)}(\beta)\left[d_{1,0}^{(2)}(\beta)\right]^2 \propto \sin^2\beta\sin^2 2\beta, \tag{36}$$

where $d_{m,n}^{(2)}$ are the rank-2 reduced Wigner rotation matrix elements. Hence this contribution has a consistent sign and is largest when the crystallite is oriented such that the dipolar tensor is at the magic angle with respect to the rotor axis (dropping to zero at $\beta = 0$ and $\beta = \pi/2$). This maximum splitting under Lee-Goldburg decoupling evaluates to

$$\Delta_{\mathrm{LG,max}}^{\mathrm{III}} = 0.0285\frac{D^3}{\nu_{\mathrm{rf}}^2}. \tag{37}$$

These correction terms have been determined for the case of simple Lee-Goldburg decoupling, while FSLG,[5] or its on-resonance implementation, PMLG,[6] is commonly used experimentally. Given the high order of these correction terms, and the additional time dependence introduced by frequency switching, it is not obvious that the correction terms for FSLG decoupling are simply related to those deduced above. Moreover, the cancellation of the second-order terms, Eq. (28), associated with the frequency switching of FSLG decoupling may not be perfect under MAS conditions since the Hamiltonian is changing over the duration of the RF period.

These questions are explored in Fig. 3, which compares the predicted splitting in the ^{13}C spectrum under LG decoupling from Eq. (31) with numerical simulations of both LG and FSLG decoupling under 10 kHz MAS (see Sec. IV for full simulation details). The predictions of Eq. (37) agree perfectly (within 1%) with the numerical simulations using LG decoupling, and the splitting under FSLG observed in the simulations has the same functional dependence on D^3/ν_{rf}^2. Somewhat counterintuitively, the splitting under FSLG decoupling is about a factor of two *larger* than under simple Lee-Goldburg decoupling. However, the frequency switching is designed to remove terms from the average Hamiltonian that are odd-order with respect to the RF, and this does not imply that other terms are also reduced. Since the J coupling is zero, the second-order contribution to the splitting, Eq. (28), is identically zero in the absence of a ^{1}H CSA.

To verify that the second-order terms are generally small, Fig. 3 also shows the results when a 2 kHz CSA (corresponding to 4 ppm at 500 MHz ^{1}H frequency) is included. As expected, the second-order terms are significant for simple Lee-Goldburg decoupling and the corresponding data points (purple diamonds) do not fit to the functional dependence expected from the third-order term. However, the frequency switching almost completely eliminates the second-order terms and the corresponding data points (blue circles) largely coincide with those obtained when the CSA is zero (green triangles).

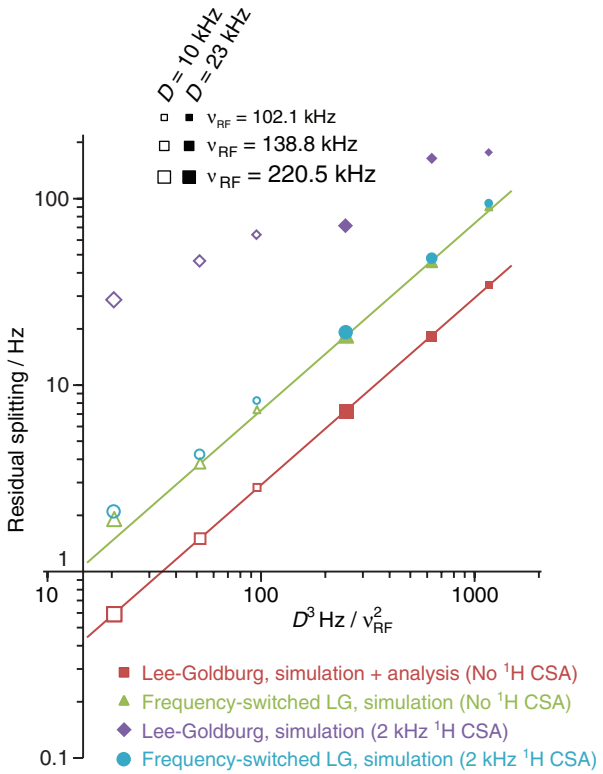

FIG. 3. Residual splitting in the simulated ^{13}C spectrum for a ^{13}C,^{1}H spin pair under 10 kHz MAS (with $J = 0$) using a single crystallite orientation at $\beta = \theta_{\mathrm{m}}$ as a function of D^3/ν_{rf}^2 for FSLG (green triangles) and LG (red squares) decoupling, evaluated for two values of D, 10 kHz (open symbols) and 23 kHz (filled symbols), and three values of ν_{rf} (reflected in the size of the symbols). The predictions of Eq. (37) lie within the size of LG symbols. Also shown are the results of simulations including a 2 kHz ^{1}H CSA with FSLG (blue circles) and LG (purple diamonds) decoupling. Unit gradient lines drawn through the symbols confirm the predicted functional dependence.

Although this analysis has been carried out for the relatively straightforward case of Lee-Goldburg decoupling, the same principles are expected to apply to more complex homonuclear decoupling schemes, such as the eDUMBO sequence used in the experimental example in Fig. 2 above. This is confirmed by the simulations shown later in Fig. 7. Moreover, simulations of eDUMBO decoupling (results not shown) confirmed that it too was extremely effective in suppressing the second-order terms associated with the ^{1}H CSA. Note that the deviation may be much larger if decoupling RF is applied to spins such as ^{19}F with much larger CSAs or where the RF and MAS cycle times have similar durations, cf. Fig. 9.

IV. NUMERICAL SIMULATIONS

Numerical simulations of heteronuclear spin systems under MAS and homonuclear decoupling have been used to confirm the predictions of the theoretical analysis. Two different simulation packages were used, pNMRsim[47] (Durham) and SPINEVOLUTION[48] (Warwick), with the two codes producing identical results in test cases. The principal model used was a two-spin ^{1}H,^{13}C system using heteronuclear dipolar and J coupling constants of $D = 23$ kHz and $J = 150$ Hz, respectively, with the principal axis of the dipolar coupling (corresponding to the internuclear axis) defining the molecular frame of reference. Unless otherwise stated, the ^{1}H shift was at 5.9 ppm with respect to the transmitter frequency (corresponding to a transmitter offset of 2.9 kHz at a 500 MHz ^{1}H Larmor frequency), which matches the experimental conditions of Fig. 1(c). In the minority of simulations that included a ^{1}H CSA, this had an anisotropy of 2 kHz (corresponding to 4 ppm at 500 MHz ^{1}H frequency), zero asymmetry, and was co-linear with the ^{13}C,^{1}H dipolar coupling.

A. Observation via ^{1}H

^{1}H spectra under FSLG decoupling were simulated under magic-angle spinning at 10 kHz. RF nutation frequencies were chosen such that the cycle periods of the FSLG decoupling and the sample spinning were commensurate over a small number of rotation periods, with the NMR signal observed once per base Lee-Goldburg cycle. This "synchronisation" allows the evolution to be calculated efficiently.[49] The powder sampling was performed over a 150 α, β and γ angle set according to a Zhang-Cheng-Wolfsberg (ZCW) scheme.[50,51] Although the two-spin Hamiltonian is invariant to the powder α angle, the ZCW integration schemes are still effective even if the integration is independent of one or more of the integration parameters. The starting state was ^{1}H magnetisation along the y axis, perpendicular to the spin-lock axis of the FSLG decoupling. The tilted axis precession created strong quadrature artifacts which were discarded in processing. Decoupling/spinning sidebands were generally of low intensity and are not shown. Full spectra were obtained via Fourier transformation of the time-domain signal after a 30 Hz Lorentzian line-broadening.

Figure 4(a) shows the significant effect of including the heteronuclear dipolar coupling in the simulations, compared to the simple scaled J doublet obtained when only the J coupling between ^{13}C and ^{1}H is included. In addition to obscuring the J doublet, the peak maximum of the resulting asymmetric lineshape is displaced from the expected scaled resonance frequency (at 1.67 kHz). Fig. 4(b) shows how this lineshape arises from the sum of individually symmetrically split spectra, and that the asymmetry arises from subtle variations in the scaled isotropic frequency with crystallite orientation. The magnitude of the apparent shifts are consistent with those observed experimentally in Fig. 1. Note that the detailed lineshape observed depends on the ^{1}H chemical shift parameters, including its anisotropy (here zero), but overall linebroadening is largely independent of the ^{1}H shift parameters (see also Fig. 5).

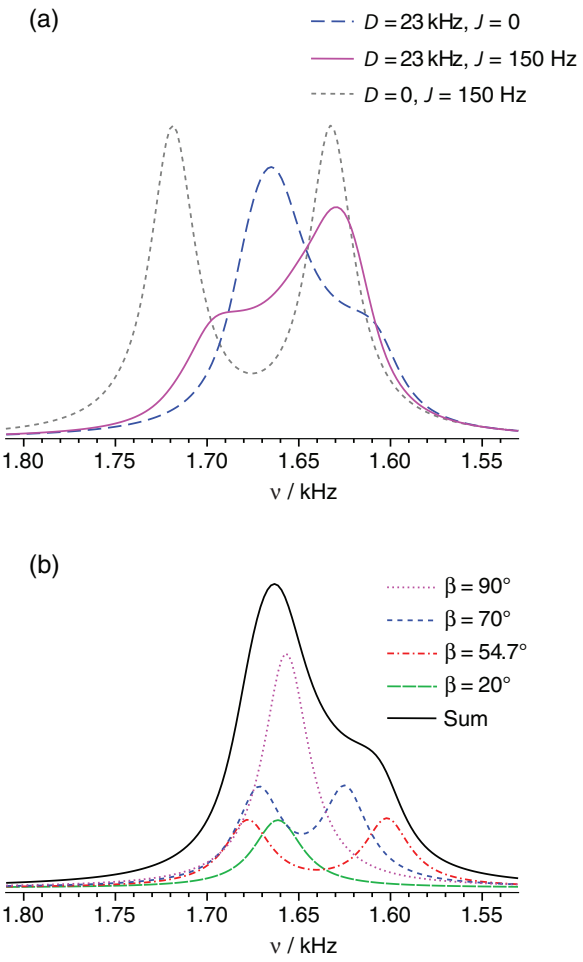

FIG. 4. Simulated ^{1}H spectra under 102.06 kHz FSLG decoupling and 10 kHz MAS. (a) Powder-averaged lineshapes obtained with $D = 23$ kHz, $J = 0$ (long dash); $D = 23$ kHz, $J = 150$ Hz (solid), and (for reference) the spectrum with only the J coupling included (short dash). (b) Powder pattern observed with $D = 23$ kHz, $J = 0$ (solid), and a representative set of spectra as a function of the β powder angle (integrated over the γ angle in 8 steps and scaled by the sin β integration weighting factor).

Figure 5 shows the effect of the offset from resonance, Ω_I, on the observed lineshape. Note how at non-zero offsets, the maximum peak intensity is distorted away from the expected peak position (shown by the reference line in grey), as observed in the experimental HETCOR spectra, Fig. 1. As anticipated in Sec. III B, the distortion of the ideal J doublet is reduced significantly in the limit $\Omega_I = 0$ since the distortion of the scaling factor described by Eq. (35) is then zero.

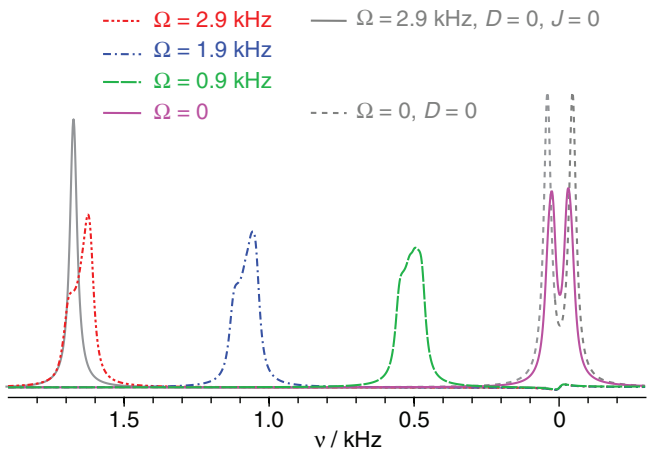

FIG. 5. Simulated ^{1}H spectra under FSLG decoupling as a function of resonance offset, Ω_I ($D = 23$ kHz, $J = 150$ Hz, 10 kHz MAS, RF nutation frequency 102.06 kHz). The two normalised reference spectra show the simulated spectrum at the maximum offset, but with zero couplings (solid grey line) and the on-resonance case (grey dashed line) in the absence of just the dipolar coupling.

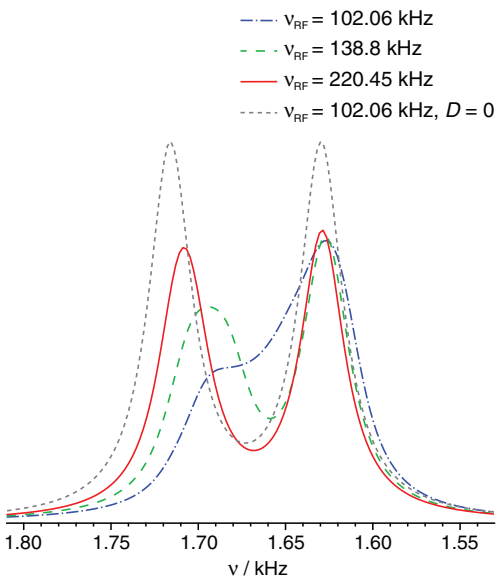

FIG. 6. Simulated ^{1}H spectra under FSLG decoupling as a function of the ^{1}H nutation frequency ($D = 23$ kHz, $J = 150$ Hz, 10 kHz MAS). The RF nutation frequencies used correspond to synchronisation conditions, τ_r/τ_c, of 25/4 (102.06 kHz), 17/2 (138.8 kHz) and 27/2 (220.45 kHz), where τ_r and τ_c are the durations of the rotor period and full FSLG cycle period, respectively.

The broadening due to the modulation of the effective splitting described by Eq. (34) remains, as shown by the difference between the spectrum for $\Omega_I = 0$ and the reference spectrum (grey dashed line) in which the heteronuclear dipolar coupling is absent. The $\Omega_I < J$ limit is not, however, a practically useful regime, particularly as it has been demonstrated both experimentally and theoretically that optimal resolution (and reduced artifact complications) is often obtained by careful positioning of the spectrum off-resonance with respect to the transmitter frequency.[9,52]

A more effective strategy to minimise these interactions is to increase the ^{1}H nutation frequency so that it significantly exceeds the strength of the heteronuclear couplings. As shown in Fig. 6, the simulated spectrum converges towards the ideal scaled J doublet in the limit $\nu_{rf}/D > 10$. However, increasing RF nutation frequencies is not without practical difficulties, not least the RF power handling limits of NMR probes. Moreover it is frequently observed that the experimental performance of current homonuclear decoupling techniques tends to decrease at high RF powers,[49] with ν_{RF} values about 100 kHz often being used in practice. The results shown in Fig. 6 are a strong incentive for developing decoupling strategies and/or probe technologies that are more effective at higher ^{1}H nutation frequencies.

B. Observation via ^{13}C

With the exception of the frequency-domain calculations presented in Figs. 3 and 9, the ^{13}C simulations were performed using SPINEVOLUTION,[48] using the same parameters for two-spin calculations as described above. Simulations to evaluate the effects of the ^{1}H homonuclear coupling were also performed using an 8 spin ^{13}C^{1}H$_7$ model system constructed using the co-ordinates of L-alanine (taken from Cambridge Structural Database reference code LALNIN23) after refinement of H atom positions using a DFT-based quantum code (GAUSSIAN03). The optimised C$_\alpha$H bond distance was 1.095 Å, corresponding to a ^{13}C,^{1}H heteronuclear dipolar coupling of 23 kHz. The additional six protons used in the model system were taken from the NH_3^+ and CH_3 hydrogen positions. The ^{1}H nuclei of the CH_3 were assumed to be in fast exchange, although including the motional averaging within the CH_3 (and/or within the NH_3^+) only modified the overall dephasing rates and did not significantly affect the results observed. The isotropic chemical shifts were chosen to match those found experimentally in L-alanine, with the ^{1}H$_\alpha$ resonance at +2.1 kHz relative to the ^{1}H transmitter frequency (corresponding to 3.5 ppm at a ^{1}H Larmor frequency of 600 MHz). Powder averaging was performed using 100 α and β powder angle pairs chosen using the REPULSION averaging scheme[53] and 16 equally stepped γ angles. The magnitude of the ^{13}C signal at the end of the τ-π-τ spin-echo period was calculated. FSLG simulations used an RF nutation frequency of 102.06 kHz and an MAS frequency of 10 kHz, over 128 time points using a τ increment of 400 μs (i.e., 4 rotor periods). eDUMBO-1$_{22}$ simulations used an RF nutation frequency of 150 kHz, an RF cycle period of 32 μs (320 steps of 100 ns), an MAS frequency of 20.833 kHz, and a τ increment of 96 μs (i.e., 3 RF periods). Where Fourier transforms of the spin-echo curves are presented, an apodisation corresponding to a line broadening of 30 Hz was applied prior to zero-filling and Fourier transformation using GSIM.[54]

Figure 7 confirms the significant interaction between the heteronuclear dipolar coupling and homonuclear decoupling using simulated spin-echo decay curves for the model ^{13}C,^{1}H spin system. In the absence of the dipolar coupling, the effect of the decoupling RF is simply to scale the effective coupling strength, leading to a slower oscillation in comparison to that observed in the absence of RF. Note that the heteronuclear coupling has no observable effect in the absence of RF, since the echo periods are integer multiples of the rotation period. However, the evolution is strongly damped when both

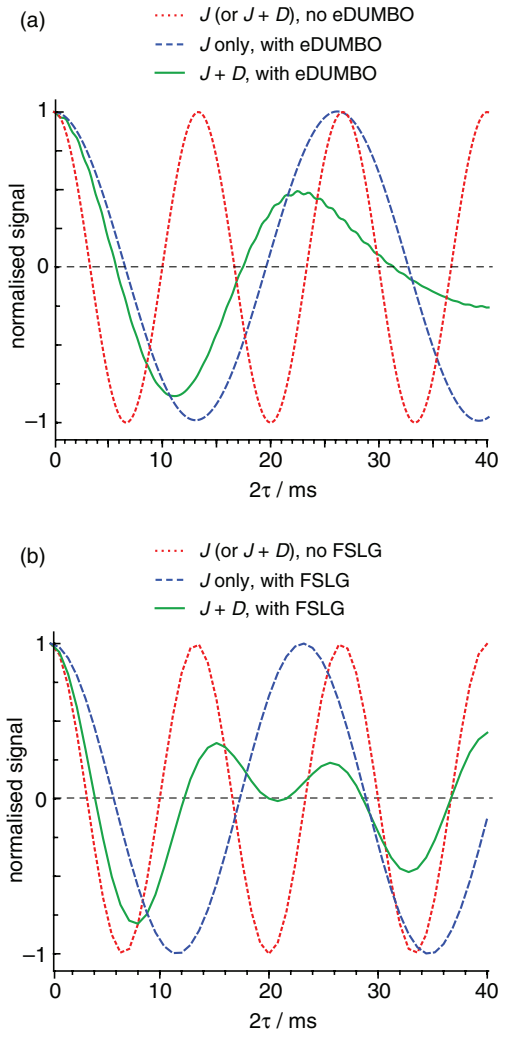

FIG. 7. Simulated ^{13}C spin-echo (τ-π-τ) curves for a model two-spin ^{13}C^{1}H system for (a) eDUMBO-1_{22} decoupling using $\nu_{rf} = 150$ kHz ($\tau_c = 32$ μs) and $\nu_r = 20.8$ kHz, and (b) FSLG decoupling using $\nu_{rf} = 102.06$ kHz and 10 kHz MAS. The red dotted lines show the evolution under the J coupling when no homonuclear decoupling is applied; the blue dashed lines show the slower evolution under the scaled J coupling when homonuclear decoupling is included. The green solid line shows the damping of the oscillation when the heteronuclear ^{13}C^{1}H coupling (D) is included.

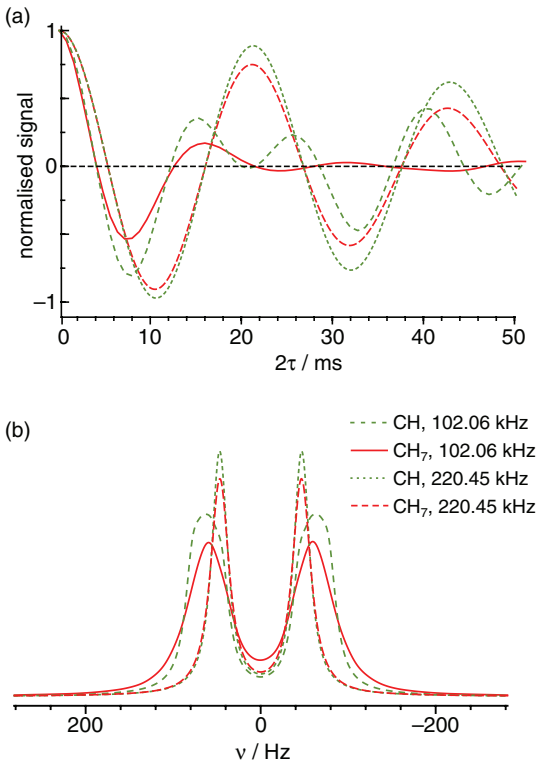

FIG. 8. (a) Simulated ^{13}C τ-π-τ spin-echo curves and (b) their Fourier transforms, simulated for FSLG homonuclear decoupling at an MAS frequency of 10 kHz and RF nutation frequencies of 102.06 kHz ($25\tau_c = 4\tau_r$) and 220.45 kHz ($27\tau_c = 2\tau_r$). Two model spin systems were used: the basic two-spin CH system and the larger CH_7 system modelled on the CH_α environment of L-alanine.

the heteronuclear dipolar coupling and the homonuclear decoupling is present. Identical trends are observed for FSLG and eDUMBO decoupling.

Focussing on FSLG decoupling, since this is more readily analysed, Fig. 8 illustrates the effect of changing the RF nutation frequency and the presence or absence of ^{1}H homonuclear couplings. Fig. 8(b) shows the corresponding Fourier transformations of the spin-echo curves in (a) (after apodisation). Those "spin-echo spectra" obtained at modest RF ($\nu_{rf} = 102$ kHz) show similar lineshape distortions to those observed in the simulated ^{1}H spectra in Figs. 4–6 above, with the exception that the lineshapes are necessarily symmetrical. In line with the predictions above, the distortions are strongly reduced as the RF nutation frequency is increased. Fig. 8 also suggests that the presence of the ^{1}H homonuclear dipolar coupling network has a relatively minor effect. In particular, there is negligible difference in the positions of the zero crossings (and hence any fitted oscillation frequency) between the results from the CH and the model CH_7 system. As might be expected, the additional homonuclear couplings damp the spin-echo decay, but without modifying the effective oscillation frequencies. This confirms the appropriateness of the two-spin model used above.

The theoretical analysis predicts that the effects observed are essentially independent of MAS frequency, provided that "resonance conditions" between ν_r and ν_{rf} are avoided. This is illustrated in Fig. 9, which shows the residual splitting in the NMR spectrum for a single crystallite (determined from the frequency difference between the two centreband transitions) as a function of MAS frequency at a fixed RF nutation frequency. The ^{1}H nutation frequency was fixed at 100 kHz and the exact values of the MAS frequency chosen to achieve "synchronisation" between RF and MAS cycle times, as discussed above. The ^{13}C,^{1}H spin pair was oriented with the internuclear vector at the magic angle with respect to the rotor axis, which corresponds to the maximal splitting (as shown in Sec. III). These calculations were performed (using PNMRSIM) directly in the frequency domain,[55] which is feasible due to the synchronisation of the RF and rotation cycle periods.

The residual splitting is independent of MAS frequency in the quasi-static limit, $\nu_{rf} \gg \nu_r$. It is important to note, however, that the effects observed here are particular to MAS spectra; it would, in any case, be impossible to resolve the

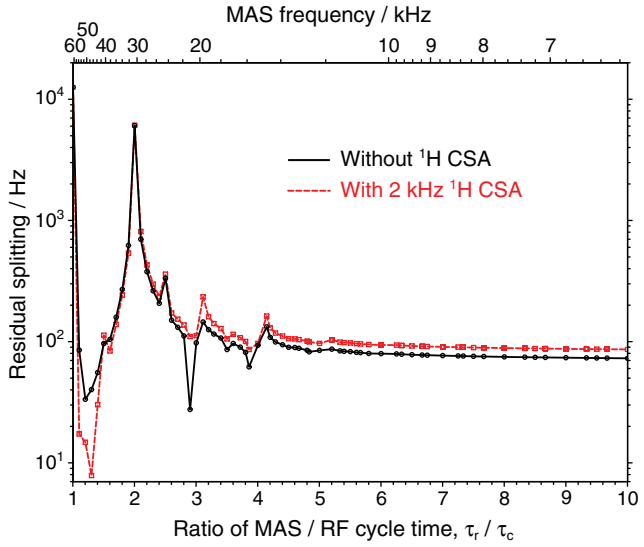

FIG. 9. Residual splitting as a function of MAS frequency in the simulated ^{13}C spectrum for a ^{13}C,^{1}H spin pair (with $J = 0$) using a single crystallite orientation at $\beta = \theta_m$ ($D = 23$ kHz, $\nu_{rf} = 100$ kHz FSLG decoupling). Data points connected by the red dashed and black solid lines correspond to simulations with and without a 2 kHz ^{1}H chemical shift anisotropy.

heteronuclear J coupling in the presence of a dominant dipolar coupling in a static sample. The key issue is that in an intermediate regime, in which neither the MAS nor the RF irradiation is sufficient to average out the dipolar coupling, the interaction between the RF and the time-dependent coupling creates measurable third-order cross terms. The presence of a ^{1}H chemical shift anisotropy (red data points) has little effect (away at least from the resonance conditions), showing that the conclusions drawn from Fig. 3 on the efficiency of averaging of second-order terms by the frequency switching are generally true.

As the ratio of RF nutation frequency to MAS frequency (τ_r/τ_c) decreases, "resonance conditions" are observed at certain ratios of the two cycle periods. Since this simulation does not include homonuclear couplings, these are not directly related to the interactions between MAS and homonuclear decoupling that have been extensively analysed[41,56] and previously observed in *multi-spin* simulations[49] in the context of ^{1}H homonuclear decoupling. For example the features shown here at $\tau_r/\tau_c = 2.9$ and 3.9 are not simple rotational resonances, and are particular to the single orientation considered. These conditions have not been investigated further since they are unlikely to be of practical significance.

V. DISCUSSION

Given that the effects described have an observable impact on widely used solid-state NMR experiments, and will apply to any experiments involving ^{13}C nuclei close to ^{1}H subject to RF, it is initially surprising that they have not been previously documented. It is commonly assumed, however, that the heteronuclear dipolar coupling has little effect on the evolution of the ^{1}H spin system under homonuclear decoupling and magic-angle spinning. In the absence of RF, the effect of the heteronuclear dipolar coupling refocuses over a rotation period; it behaves "inhomogeneously" in the terminology of Maricq and Waugh.[57] Hence the ^{1}H dimension of heteronuclear correlation experiments using fast MAS alone for resolution are unperturbed by the ^{13}C,^{1}H dipolar couplings. However, the nuclear spin Hamiltonian no longer behaves inhomogeneously in the presence of RF, even in the case of a spin pair, and the ^{13}C,^{1}H dipolar coupling is no longer so benign. But given the general complications of calibrating the ^{1}H shift scale introduced by homonuclear decoupling, it is perhaps unsurprising that small perturbations in the apparent chemical shift could go unnoticed. Similarly, the relatively rapid dephasing of ^{13}C magnetisation under homonuclear decoupling could be dismissed as the result of sub-optimal decoupling performance. As shown in Fig. 1, only careful comparison of apparent ^{1}H shifts reveals discrepancies between values observed via short-range correlations (where the local spin system contains a large ^{13}C,^{1}H coupling) and long-range correlations (where the heteronuclear couplings are much weaker). The size of the ^{13}C,^{1}H dipolar coupling for a direct CH bond (about 25 kHz) in comparison with the RF nutation frequencies typically used for homonuclear decoupling (about 100 kHz) means that its effects are of the order of 100 Hz and cannot be ignored. Other NMR nuclei with lower magnetogyric ratios than ^{13}C, such as ^{15}N will be significantly less affected since the effects scale as γ^3.

The interaction between heteronuclear dipolar couplings and RF irradiation has been extensively discussed in the context of *heteronuclear* decoupling.[30,35,37] A variety of techniques have been used to probe the effective Hamiltonians under continuous wave RF decoupling in small systems subject to magic-angle spinning, for example, in pure dipolar systems.[33] In particular, the cross-term arising between the heteronuclear dipolar coupling and the ^{1}H chemical shift anisotropy has been shown to be particularly important in describing decoupling performance.[32,37] Similarly, the presence of strong heteronuclear dipolar couplings to third nuclei, such as ^{19}F, has been shown to degrade decoupling performance in both static and spinning examples by effectively pushing the irradiation off-resonance (static samples)[58] or increasing the effective CSA/dipolar cross-term in spinning samples.[59] However, none of the previous work has described the third-order dipolar cross-term discussed here, for the simple reason that the correction term of Eq. (31) is zero for on-resonance irradiation ($\theta = 0$). Although applied here to homonuclear decoupling, the analysis above essentially generalises previous work considering heteronuclear decoupling using on-resonance RF irradiation.

Mitigating these effects would improve ^{1}H resolution and the reliability of ^{1}H chemical shifts under homonuclear decoupling. The efficiency of coherence transfer using J couplings would also be significantly improved, cf. Fig. 8 (although quantitative measurements of small J values will still be slightly distorted by the effects described). In principle, it is possible to use rotation-synchronised irradiation schemes[60] that suppress the anisotropic components of the heteronuclear couplings while retaining the isotropic component of the heteronuclear J interaction.[61] However, these sequences are derived using average Hamiltonian theory on the assumption

that the RF is the dominant term in the Hamiltonian. Preliminary simulations using the "R-sequences" given in Ref. 61 and R elements optimised for broadband inversion,[62] showed no significant improvement in lineshape over conventional FSLG decoupling that does not attempt to suppress the anisotropic component of the heteronuclear couplings.

The ideal solution is to develop decoupling strategies that are effective at high nutation frequencies; the distortions in the ^{1}H spectrum are minimal at nutation frequencies around 200 kHz, cf. Fig. 6. It is interesting to note in this context that conventional strategies used to improve the performance of homonuclear decoupling, such as frequency switching, may work against the suppression of this heteronuclear dipolar cross-term, cf. Fig. 3. Given the difficulty of analysing such high-order terms via analytical approaches, numerical simulation and direct on-spectrometer optimisation[27,63] will have an important role to play in devising improved strategies. Additional theoretical work is also required for the increasingly significant regime in which the MAS rate exceeds the RF nutation frequency,[64] where the analysis described is no longer applicable.

ACKNOWLEDGMENTS

A.T. thanks Engineering and Physical Sciences Research Council (EPSRC) and GlaxoSmithKline for support (CASE Ph.D). I.F. was supported under EPSRC Grant No. EP/H023291. The authors thank Professor Robin Harris (Emeritus) for drawing their attention to the discordant ^{1}H shifts in HETCOR spectra. Helpful discussions with Dr. Tran Pham and Dr. Frederick Vogt (GlaxoSmithKline) are acknowledged.

[1] V. E. Zorin, S. P. Brown, and P. Hodgkinson, J. Chem. Phys. **125**, 144508:1 (2006).
[2] M. Lee and W. I. Goldburg, Phys. Rev. **140**, 1261 (1965).
[3] J. S. Waugh, L. M. Huber, and U. Haeberlen, Phys. Rev. Lett. **20**, 180 (1968).
[4] B. C. Gerstein, R. G. Pembleton, R. C. Wilson, and L. M. Ryan, J. Chem. Phys. **66**, 361 (1977).
[5] A. Bielecki, A. C. Kolbert, and M. H. Levitt, Chem. Phys. Lett. **155**, 341 (1989).
[6] E. Vinogradov, P. K. Madhu, and S. Vega, Chem. Phys. Lett. **314**, 443 (1999).
[7] D. Sakellariou, A. Lesage, P. Hodgkinson, and L. Emsley, Chem. Phys. Lett. **319**, 253 (2000).
[8] P. K. Madhu, Solid State Nucl. Magn. Reson. **35**, 2 (2009).
[9] P. Hodgkinson, Annu. Rev. NMR Spectrosc. **72**, 185 (2011).
[10] A. Lesage, D. Sakellariou, S. Steuernagel, and L. Emsley, J. Am. Chem. Soc. **120**, 13194 (1998).
[11] B.-J. van Rossum, C. P. de Groot, V. Ladizhansky, S. Vega, and H. J. M. de Groot, J. Am. Chem. Soc. **122**, 3465 (2000).
[12] A. Lesage, L. Emsley, F. Penin, and A. Böckmann, J. Am. Chem. Soc. **128**, 8246 (2006).
[13] F. Hempelmann, S. Hölper, M.-K. Verhoefen, A. C. Woerner, T. Köhler, S.-A. Fiedler, N. Pfleger, J. Wachtveitl, and C. Glaubitz, J. Am. Chem. Soc. **133**, 4645 (2011).
[14] R. K. Harris, S. Cadars, L. Emsley, J. R. Yates, C. J. Pickard, R. K. R. Jetti, and U. J. Griesser, Phys. Chem. Chem. Phys. **9**, 360 (2007).
[15] E. Salager, R. S. Stein, C. J. Pickard, B. Elena, and L. Emsley, Phys. Chem. Chem. Phys. **11**, 2610 (2009).
[16] F. Blanc, R. Berthoud, C. Copéret, A. Lesage, L. Emsley, R. Singh, T. Kreickmann, and R. R. Schrock, Proc. Natl. Acad. Sci. U.S.A. **105**, 12123 (2008).
[17] J. W. Wiench, C. Michon, A. Ellern, P. Hazendonk, A. Iuga, R. J. Angelici, and M. Pruski, J. Am. Chem. Soc. **131**, 11801 (2009).
[18] L. Mafra, J. Rocha, C. Fernandez, and F. A. A. Paz, J. Magn. Reson. **180**, 236 (2006).
[19] C. Steinbeck, M. Ernst, B. Meier, and B. Chmelka, J. Phys. Chem. C **112**, 2565 (2008).
[20] J. R. Yates, T. N. Pham, C. J. Pickard, F. Mauri, A. M. Amado, A. M. Gil, and S. P. Brown, J. Am. Chem. Soc. **127**, 10216 (2005).
[21] M. Hušák, A. Jegorov, J. Brus, W. van Beek, P. Pattison, M. Christensen, V. Favre-Nicolin, and J. Maixner, Struct. Chem. **19**, 517 (2008).
[22] A. Lesage, S. Steuernagel, and L. Emsley, J. Am. Chem. Soc. **120**, 7095 (1998).
[23] B. Elena, A. Lesage, S. Steuernagel, A. Böckmann, and L. Emsley, J. Am. Chem. Soc. **127**, 17296 (2005).
[24] A. Lesage, L. Emsley, M. Chabanas, C. Copéret, and J.-M. Basset, Angew. Chem., Int. Ed. **41**, 4535 (2002).
[25] R. K. Harris, P. Hodgkinson, V. Zorin, J.-N. Dumez, B. Elena, L. Emsley, E. Salager, and R. Stein, Magn. Reson. Chem. **48**, S103 (2010).
[26] D. C. Apperley, A. S. Batsanov, S. J. Clark, R. K. Harris, P. Hodgkinson, and D. B. Jochym, "Computation of magnetic shielding to simultaneously validate a crystal structure and assign a solid-state NMR spectrum," J. Mol. Struct. (in press).
[27] B. Elena, G. De Paëpe, and L. Emsley, Chem. Phys. Lett. **398**, 532 (2004).
[28] B. M. Fung, A. K. Khitrin, and K. Ermolaev, J. Magn. Reson. **142**, 97 (2000).
[29] J. M. Griffin, C. Tripon, A. Samoson, C. Filip, and S. P. Brown, Magn. Reson. Chem. **45**, S198 (2007).
[30] P. Hodgkinson, Prog. Nucl. Magn. Reson. Spectrosc. **46**, 197 (2005).
[31] J. S. Waugh, J. Magn. Reson. **50**, 30 (1982).
[32] M. Ernst, S. Bush, A. C. Kolbert, and A. Pines, J. Chem. Phys. **105**, 3387 (1996).
[33] J. R. Sachleben, J. Gaba, and L. Emsley, Solid State Nucl. Magn. Reson. **29**, 30 (2006).
[34] I. Scholz, B. H. Meier, and M. Ernst, J. Chem. Phys. **127**, 204504 (2007).
[35] I. Scholz, P. Hodgkinson, B. H. Meier, and M. Ernst, J. Chem. Phys. **130**, 114510:1 (2009).
[36] I. Scholz, J. D. van Beek, and M. Ernst, Solid State Nucl. Magn. Reson. **37**, 39 (2010).
[37] M. Ernst, J. Magn. Reson. **162**, 1 (2003).
[38] M. Leskes, P. Madhu, and S. Vega, Prog. Nucl. Magn. Reson. Spectrosc. **57**, 345 (2010).
[39] J. R. Sachleben, S. Caldarelli, and L. Emsley, J. Chem. Phys. **104**, 2518 (1996).
[40] R. Ramesh and M. S. Krishnan, J. Chem. Phys. **114**, 5967 (2001).
[41] E. Vinogradov, P. K. Madhu, and S. Vega, J. Chem. Phys. **115**, 8983 (2001).
[42] M. Ernst, A. Samoson, and B. H. Meier, J. Chem. Phys. **123**, 064102 (2005).
[43] R. Ramachandran and R. G. Griffin, J. Chem. Phys. **122**, 164502 (2005).
[44] R. Ramachandran, V. S. Bajaj, and R. G. Griffin, J. Chem. Phys. **122**, 164503 (2005).
[45] M. B. Monagan, K. O. Geddes, K. M. Heal, G. Labahn, S. M. Vorkoetter, J. McCarron, and P. DeMarco, *Maple 10 Programming Guide* (Maplesoft, Waterloo, ON, Canada, 2005).
[46] P. W. Atkins, *Molecular Quantum Mechanics*, 2nd ed. (Oxford University Press, New York, 1983).
[47] P. Hodgkinson, "pNMRsim: a general simulation program for large problems in solid-state NMR," http://www.durham.ac.uk/paul.hodgkinson/pnmrsim.
[48] M. Veshtort and R. G. Griffin, J. Magn. Reson. **178**, 248 (2006).
[49] V. E. Zorin, M. Ernst, S. P. Brown, and P. Hodgkinson, J. Magn. Reson. **192**, 183 (2008).
[50] S. K. Zaremba, Ann. Mat. Pura Appl. **73**, 293 (1966).
[51] H. Conroy, J. Chem. Phys. **47**, 5307 (1967).
[52] M. Leskes, P. K. Madhu, and S. Vega, J. Chem. Phys. **125**, 124506 (2006).
[53] M. Bak and N. C. Nielsen, J. Magn. Reson. **125**, 132 (1997).
[54] V. Zorin, "GSIM — a visualisation and processing program for solid-state NMR," http://gsim.sourceforge.net.
[55] P. Hodgkinson and L. Emsley, Prog. Nucl. Magn. Reson. Spectrosc. **36**, 201 (2000).
[56] E. Vinogradov, P. K. Madhu, and S. Vega, Chem. Phys. Lett. **329**, 207 (2000).
[57] M. M. Maricq and J. S. Waugh, J. Chem. Phys. **70**, 3300 (1979).
[58] G. Antonioli, D. E. McMillan, and P. Hodgkinson, Chem. Phys. Lett. **344**, 68 (2001).
[59] G. Antonioli and P. Hodgkinson, J. Magn. Reson. **168**, 124 (2004).

[60]M. H. Levitt, in *Encyclopaedia of Nuclear Magnetic Resonance*, edited by D. M. Grant and R. K. Harris (Wiley, New York, 2002).
[61]P. K. Madhu, X. Zhao, and M. H. Levitt, Chem. Phys. Lett. **346**, 142 (2001).
[62]R. Freeman, *Spin Choreography* (Spektrum Academic, Oxford, 1996).
[63]G. De Paëpe, P. Hodgkinson, and L. Emsley, Chem. Phys. Lett. **376**, 259 (2003).
[64]M. Ernst, A. Samoson, and B. H. Meier, Chem. Phys. Lett. **348**, 293 (2001).
[65]See supplementary material at http://dx.doi.org/10.1063/1.3684879 for details of the spin-echo measurements and fitting, sample pNMRsim and SPINEVOLUTION input files for numerical simulations and the MAPLE™ worksheet for analytical calculations.